EES Solar

REVIEW

View Article Online
View Journal | View Issue

Cite this: *EES Sol.*, 2025, **1**, 670

How to design active sites for tailoring the C_1 and C_2 products of CO_2 photoreduction

Peijin Du,†[a] Suning Zhang,†[a] Jinyu Ding, †[a] Dongpo He,[a] Qinyuan Hu,[a] Xingchen Jiao *[a] and Yi Xie *[b]

Received 29th May 2025
Accepted 21st July 2025

DOI: 10.1039/d5el00082c

rsc.li/EESSolar

Photocatalytic CO_2 reduction generally involves three fundamental stages: light absorption, charge carrier separation, and the redox reactions occurring on the surface. Adjusting these processes to optimize the activity and selectivity of CO_2 photoreduction towards C_1 and C_2 products has proven to be an effective strategy. In this review, we summarize the design of active sites through various structural modifications, including defect structure, metal doping structure, heterojunction structure, alloy structure, loading structure, and composite structure, to tailor the product selectivity and activity of CO_2 photoreduction. Additionally, we provide a concise overview and outlook on strategies for stabilizing active sites, constructing bio-inorganic systems, and elucidating catalytic mechanisms.

Broader context

Due to the burning of fossil fuels and industrial activities, atmospheric carbon dioxide concentrations have risen to critical levels, significantly impacting global climate change. Solar-driven conversion of CO_2 into C_1 or C_2 products (such as methane, methanol or ethylene) represents a promising sustainable technology that mimics natural photosynthesis, transforming sunlight, water, and CO_2 into energy-rich molecules. This process involves three key steps: the absorption of light, the separation of charge carriers, and the redox reactions occurring on the surface. Currently, photocatalysts face challenges including narrow light absorption ranges and low charge carrier separation efficiencies. Therefore, optimizing these steps by designing active sites is crucial for enhancing performance. Combining this technology with renewable energy systems further enhances its feasibility and establishes photocatalytic CO_2 reduction as a cornerstone for the future circular carbon economy and sustainable energy solutions.

1 Introduction

The Paris Agreement underscores the imperative to reduce global carbon dioxide (CO_2) emissions by 50% by the year 2030 and to achieve complete carbon neutrality by 2050.[1,2] The increment in atmospheric CO_2 concentrations has posed significant challenges, including climate change and air pollution, representing major issues of the 21st century. The

[a]*Key Laboratory of Synthetic and Biological Colloids, Ministry of Education, School of Chemical and Material Engineering, Jiangnan University, Wuxi 214122, China. E-mail: xcjiao@jiangnan.edu.cn*

[b]*State Key Laboratory of Precision and Intelligent Chemistry, University of Science and Technology of China, Hefei, Anhui 230026, China. E-mail: yxie@ustc.edu.cn*

† These authors contributed equally to this work.

From left to right: Jinyu Ding, Suning Zhang and Peijin Du

Peijin Du is currently studying for her Master's degree at Jiangnan University. Her current interests include the synthesis and characterization of two-dimensional solid materials, and their applications in photocatalytic CO_2/plastic conversion. Suning Zhang is currently pursuing a Master's degree at Jiangnan University. Her current research interests include the preparation and assembly of low-dimensional nanomaterials, as well as photocatalytic CO_2 reduction. Jinyu Ding received her Master's degree at Jiangnan University in 2025. Her current interests include the synthesis and characterization of two-dimensional metal oxides, and their applications in photo/electro-catalytic CO_2/plastic conversion into valuable fuels.

diminution of fossil fuel reserves and the exacerbation of atmospheric conditions due to excessive CO_2 emissions have propelled the scientific community to innovate alternative energy solutions to meet the escalating energy needs of the present and the future. Current methodologies for the capture and utilization of CO_2, in conjunction with emerging innovative technologies, are instrumental in facilitating the attainment of these ambitious environmental objectives.[3] The photocatalytic reduction of CO_2 and water into valuable chemicals and fuels, emulating the natural process of photosynthesis, is heralded as one of the most auspicious strategies for reducing atmospheric CO_2 levels.[4–7] This approach not only contributes to the mitigation of climate change but also facilitates the development of sustainable energy sources, thereby addressing critical environmental challenges. Harnessing solar energy, utilizing water (H_2O) as a reductant, and employing a photocatalyst, this innovative process is commonly referred to as artificial photosynthesis.[8,9] It diverges from natural photosynthesis, which occurs within the chloroplasts of plant leaves, converting the same reactants into oxygen (O_2) and glucose, by differing in both the system architecture and the end products generated. At present, the viability of solar-to-fuel conversion technology as a rival to the natural photosynthetic mechanism in terms of efficiency remains an open question. The efficiency of CO_2 photoreduction is predominantly influenced by the selection of the catalyst,[10] making it crucial to design and fabricate catalysts with superior efficiency to enhance the overall performance of the process. As such, there is a pressing need to prioritize the development of catalysts that can significantly improve the efficiency of CO_2 photoreduction.

In recent studies, CO_2 photoreduction into a variety of compounds, including carbon monoxide (CO), methane (CH_4), formic acid (HCOOH), methanol (CH_3OH), formaldehyde (HCHO), and ethanol (C_2H_5OH)—spanning both C_1 and C_2 categories—has emerged as a vibrant field of study.[11–14] This area has captivated scientific interest for several decades and necessitates deeper exploration. The targeted photoreduction of CO_2 to diverse C_1 products, such as CO, CH_4, CH_3OH, and HCOOH, is of particular interest. Typically, CO and CH_4 serve as gaseous fuels with lower calorific values, while CH_3OH and HCOOH are utilized as liquid fuels.[15,16] C_2 and higher hydrocarbons/alcohols are utilized as fuels with high calorific values and as raw materials for chemical synthesis, making the conversion of CO_2 into C_1 and C_2 or higher hydrocarbons crucial for meeting future energy and chemical needs. The directed photoreaction of CO_2 to produce C_1 or C_2 products

From left to right: Dongpo He, Qinyuan Hu

Dongpo He received his Master's degree at Dalian Polytechnic University in 2023. He is currently pursuing his PhD in the School of Chemistry and Materials Science at Jiangnan University. He mainly focuses on catalytic processes for energy and environmental applications of low-dimensional solid materials, such as the catalytic conversion of waste plastics and the photoreduction of CO_2. Qinyuan Hu received his BS degree at Jiangnan University in 2022. He is currently pursuing his PhD degree at Jiangnan University. His current interests include the synthesis and characterization of two-dimensional metal oxides and sulfides, and their applications in catalytic CO_2 and plastic conversion.

Xingchen Jiao

Xingchen Jiao received his BS degree from the Department of Chemistry at Hefei University of Technology (2014) and PhD degree in Inorganic Chemistry from the University of Science and Technology of China (2019). After that he worked as a postdoctoral fellow at the University of Science and Technology of China. In 2022, he joined Jiangnan University as a professor. His current interests include the synthesis and characterization of nanostructures, as well as their applications in CO_2 photo-/electro-conversion into hydrocarbon fuels.

Yi Xie

Yi Xie received her BS degree from Xiamen University (1988) and a PhD from the University of Science and Technology of China (USTC, 1996). She is now a full professor of the Department of Chemistry, USTC. She was appointed as the Cheung Kong Scholar Professor of inorganic chemistry in 2000 and elected as a member of the Chinese Academy of Sciences in 2013. Her research interests include cutting-edge research in four major frontiers: solid state materials chemistry, nanotechnology, energy science and theoretical physics.

holds considerable appeal and importance, particularly from both academic and industrial perspectives. In the context of a photocatalytic CO_2 reduction process, it generally involves three fundamental stages: the absorption of light, the separation of charge carriers, and the redox reactions occurring on the surface.[17–20] The complexity of multiple protonation steps during the surface redox reactions presents significant hurdles in attaining the desired specificity, as it can result in the generation of a diverse array of products. To this end, it is indeed possible to modulate these three processes to fine-tune the activity and selectivity of CO_2 photoreduction towards C_1 and C_2 products.

Owing to the significant advancements in CO_2 photoreduction in recent years, a multitude of review articles have been published, reflecting the growing interest and progress in this field.[21–23] Some of them concentrate on the criteria for selecting photocatalysts, while others delve into the underlying principles. Additionally, there are reviews that explore various strategies aimed at enhancing the performance of these photocatalytic systems.[24,25] In a distinctive departure from existing literature, we are pleased to offer a contemporary review that focuses on the design of active sites to customize the C_1 and C_2 products of CO_2 photoreduction by strategically modulating the aforementioned three processes (Scheme 1). First, we focus on strategies to improve the light absorption capacity of photocatalysts, including defect engineering and metal doping engineering, both of which have shown significant potential in boosting CO_2 photoreduction performance. Secondly, we emphasize how heterojunction engineering and alloy engineering influence the charge carrier dynamics of photocatalysts. These approaches effectively suppress electron–hole recombination and enhance charge separation efficiency, thereby facilitating the photocatalytic reduction of CO_2. Thirdly, we analyze the adsorption mode of hydrogen-containing intermediates and the role of active sites in regulating the protonation process, which critically impact the selective formation of C_1 or C_2 products. Lastly, comprehensive insights are presented on the rational design of photocatalyst active sites for the photoreduction of CO_2 into C_1 or C_2 products, along with an in-depth analysis of the challenges and practical difficulties encountered in real-world applications. This review comprehensively examines current strategies for active site engineering, elucidates critical limitations, and offers perspectives for addressing these challenges. This review serves to provide valuable guidance and practical assistance for the rational design of active sites in CO_2 photoreduction catalysts, aiming to advance the field of sustainable carbon utilization.

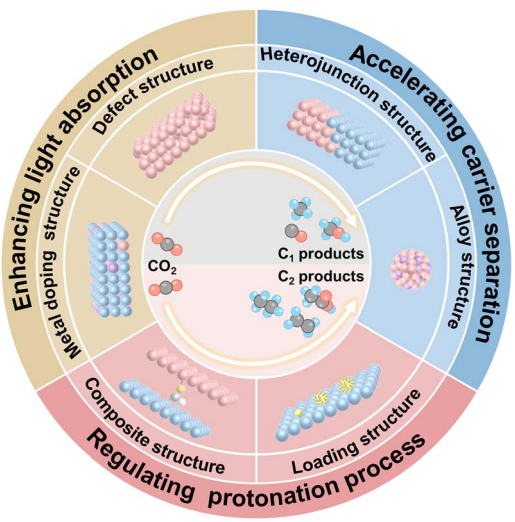

Scheme 1 Schematic illustrations of various strategies for designing active sites to tailor the C_1 and C_2 products of the CO_2 photoreduction process.

2 Design strategies for regulating the active sites of photocatalysts

It is well known that the photoreduction of CO_2 primarily involves three key processes: light absorption, charge carrier separation, and redox reactions occurring on the surface (Fig. 1). Among these, light absorption has received significant attention, particularly in the visible light region. However, infrared light, which accounts for approximately 50% of sunlight, remains underexplored and underutilized. Thus, expanding the light absorption range is an effective strategy for enhancing photocatalyst performance. Furthermore, improving the efficiency of charge carrier separation is crucial for optimizing charge transfer and increasing the yield of CO_2 photoreduction. Lastly, the regulation of the protonation process in surface redox reactions is essential for controlling the transformation of intermediates into target products, thereby achieving the desired outcomes.

2.1 Enhancing light absorption

2.1.1 Defective structure enhances light absorption. Currently, the underutilization of infrared light, which constitutes over 50% of solar radiation, remains a pressing challenge in photocatalytic CO_2 reduction.[26,27] Wide-bandgap semiconductors ensure that the theoretical potentials for CO_2 reduction and H_2O oxidation are simultaneously satisfied (Fig. 2a).[28] Furthermore, the introduction of defect structures facilitates the generation of intermediate bands, thus broadening the light absorption spectrum. Consequently, defect structures have garnered significant attention in photocatalytic CO_2 reduction due to their unique advantages.[29,30] Recently, Liang *et al.* prepared WO_3 nanosheets and demonstrated that the introduction of oxygen vacancies through various atmospheric treatments significantly altered their properties.[28] Fig. 2b illustrated the formation of varying concentrations of oxygen vacancies within the WO_3 nanosheets. These oxygen vacancies were shown in Fig. 2c to extend the light absorption range of the WO_3 nanosheets into the infrared region. This enhanced light absorption capability, ascribed to the defect structure, facilitated the photoreduction of CO_2 to CO under near-infrared irradiation (Fig. 2d). The study concluded that the introduction of defect structures, such as oxygen vacancies, created a unique charge density distribution within the

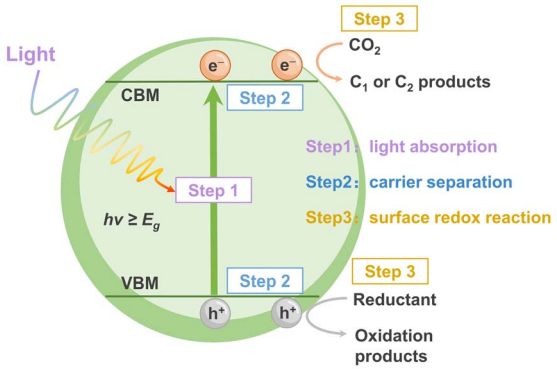

Fig. 1 Schematic diagram of the process of CO_2 photoreduction, including light absorption, charge carrier separation, and redox reactions occurring on the surface.

material. This modification not only broadened the light absorption spectrum of WO_3 nanosheets but also enhanced their overall light utilization efficiency. Additionally, Wu *et al.* also prepared BiOBr nanosheets with rich oxygen vacancies. The introduction of oxygen vacancies resulted in the formation of defect levels, which extended the light absorption range into the visible spectrum.[31] As shown in Fig. 2e, with the increase of ultraviolet light irradiation time on the pristine BiOBr nanosheets, a new absorption peak gradually appears in the visible light range. The formation of oxygen vacancies, resulting from the creation of defect structures, accounted for the strongest signal observed at $g = 2.004$ in the EPR spectra (Fig. 2f). Compared with the BiOBr nanosheets and bulk BiOBr without oxygen vacancies, the BiOBr nanosheets rich in oxygen vacancies exhibited excellent CO_2 photoreduction performance (Fig. 2g), with a CO evolution rate of approximately 87.4 μmol g^{-1} h^{-1}, which is 20 times and 24 times those of BiOBr nanosheets and bulk BiOBr, respectively. Overall, this advancement highlights the potential of defect engineering in optimizing materials for photocatalytic applications, particularly in processes like CO_2 reduction under infrared light. However, current approaches struggle to precisely regulate the types and concentrations of defects, which may lead to the formation of inactive defects or their potential filling or reconstruction during the reaction process, thus reducing catalytic efficiency.

2.1.2 Metal doping enhances light absorption. Compared with defect structures, introducing noble metal components on the substrate material can also effectively enhance the light absorption capacity.[32] This improvement arises because the doping of noble metals (such as Au, Pt, Ag) induces surface plasmon resonance effects. LSPR usually occurs on plasmonic metal nanoparticles (Au,[33] Ag[34] and Cu[35]), where resonance induced collective oscillations of electrons are formed when the frequency of the incident photons matches the frequency of the surface electric field (Fig. 3a).[36,37] Bearing the above in mind, Chen *et al.* incorporated Au, Pt, and Pd into BiOCl to investigate their co-catalytic interactions.[38] As displayed in Fig. 3b, the localized surface plasmon resonance of Au nanoparticles facilitated additional light absorption in the visible light region. Notably, the direct bandgap energy of BiOCl catalysts decreased accordingly (Fig. 3c), demonstrated that the plasmon resonance effect induced by the incorporated noble metals effectively enhanced the light harvesting ability. Moreover, the BiOCl doped with Au, Pt, and Pd exhibited superior catalytic activity in the photocatalytic reduction of CO_2 (Fig. 3d), significantly

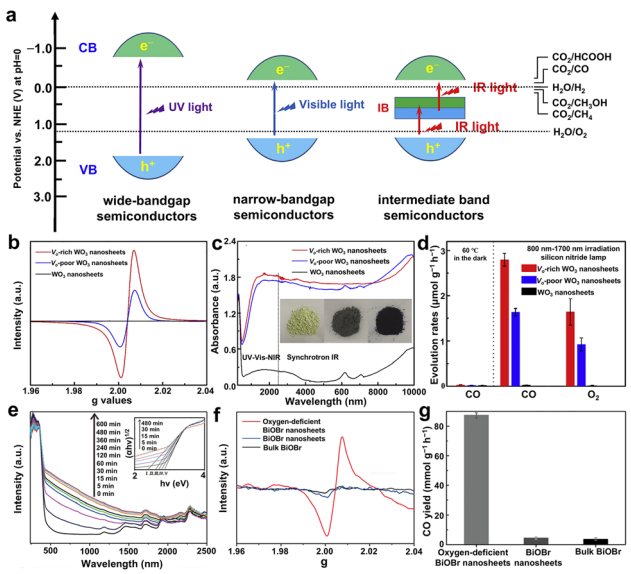

Fig. 2 (a) Energy band diagram of solar driven full decomposition of CO_2 and H_2O into hydrocarbons and O_2. (b) ESR spectra and (c) optical absorption spectra of WO_3 nanosheets. (d) CO and O_2 formation rates over WO_3 nanosheets. Reproduced with permission from ref. 28. Copyright 2018, Elsevier. (e) Optical absorption spectra for BiOBr nanosheets. (f) EPR spectra and (g) CO yield of oxygen-deficient BiOBr nanosheets, BiOBr nanosheets, and bulk BiOBr. Reproduced with permission from ref. 31. Copyright 2024, Wiley-VCH.

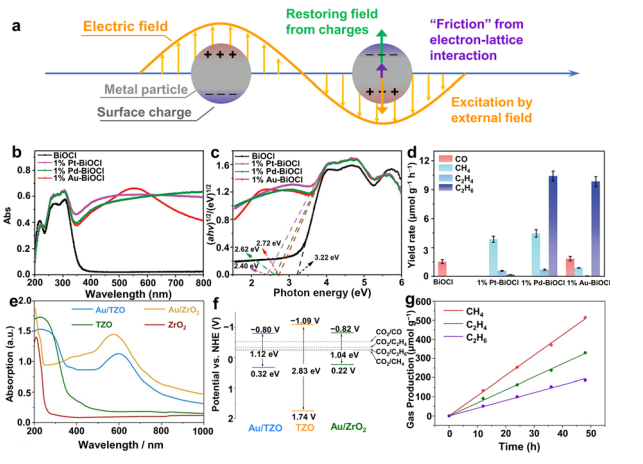

Fig. 3 (a) The formation of the localized surface plasmon resonance phenomenon on metal nanoparticles. Reproduced with permission from ref. 37. Copyright 2025, Elsevier. (b) UV-vis diffuse reflectance spectra, (c) bandgaps and (d) yields of BiOCl and 1% M/BiOCl (M = Pt, Pd, and Au) samples. Reproduced with permission from ref. 38. Copyright 2024, Wiley-VCH. (e) UV-vis absorption spectra and (f) energy level diagram for Au/TZO, Au/ZrO_2 and TZO. (g) The yield of photocatalytic CO_2 reduction by using Au/TZO as the catalyst. Reproduced with permission from ref. 39. Copyright 2025, Wiley-VCH.

promoting the conversion of CO_2 to hydrocarbons. Furthermore, Xu *et al.* developed a Zr/Ti dual-metal oxide solid solution support derived from metal–organic frameworks (MOFs), with Au nanoparticles anchored on the surface (Au/TZO), indicating significant advantages in photocatalytic CO_2 reduction to syngas.[39] As revealed in Fig. 3e, the multi-component Au/TZO exhibited strong light absorption in the range of 200–800 nm. Furthermore, the incorporation of Au nanoparticles narrowed the bandgap of TZO (Fig. 3f), and significantly improved its photocatalytic performance. When Au/TZO was employed as the photocatalyst, the predominant products were H_2 and CO. Production rates of these gases showed a linear increase with respect to the irradiation time, as illustrated in Fig. 3g. The total yields reached 271.6 μmol g^{-1} h^{-1} for H_2 and 260.6 μmol g^{-1} h^{-1} for CO, respectively. However, precious metals capable of producing the LSPR effect are hindered in practical applications due to their high costs and limited terrestrial reserves, making the search for alternative materials a significant challenge for the future. Low-cost non-precious metals offer promising application prospects. Future research can explore the construction of dual active sites using non-precious metals to reduce reliance on precious metals and lower costs.

2.2 Accelerating charge carrier separation

2.2.1 Heterojunction structure accelerates charge carrier separation. The practical application of photocatalytic CO_2 reduction is hindered by numerous challenges, with the most critical issue being the enhancement of photogenerated charge carrier separation efficiency and prevention of recombination. Recent advancements have demonstrated that heterojunction engineering is an effective strategy to address these challenges.[40,41] By constructing an interfacial electric field at the interface of two or more semiconductor materials, heterojunction engineering has proven capable of significantly improving the separation efficiency of photogenerated charge carriers,[42,43] thereby enhancing overall photocatalytic performance.[44] However, the limited interfacial contact area within the heterostructure results in reduced charge transport efficiency at the interface, which significantly hinders the improvement of photocatalytic performance from a dynamic perspective. Based on the above considerations, Yu *et al.* successfully fabricated In_2O_3/Nb_2O_5 heterojunction with intimate interfacial contact through a direct one-step electrospinning process.[45] Fig. 4a illustrated the formation process of the In_2O_3/Nb_2O_5 S-scheme heterojunction. Due to the higher Fermi level of Nb_2O_5 compared to In_2O_3, Nb_2O_5 migrated towards In_2O_3, generating an interfacial electric field (IEF) and achieving effective band alignment at the interface. Photogenerated electrons in the conduction band (CB) of In_2O_3 exhibited a preferential transfer to the valence band (VB) of Nb_2O_5 under light irradiation, where they recombine with holes. The CO_2 reduction performance of the In_2O_3/Nb_2O_5 catalyst demonstrated its outstanding photocatalytic performance, achieving a CO_2 to CO conversion yield close to 100% (Fig. 4b). Transient absorption spectra in Ar atmospheres in Fig. 4c–e revealed that the In_2O_3/Nb_2O_5 heterojunction catalyst reduced the recombination of photoelectrons and holes. Furthermore, the S-type heterojunction interfacial contact was demonstrated to significantly promote charge transfer and separation, enhancing photocatalytic efficiency. Moreover, Huang *et al.* developed a two-dimensional CuS–Bi_2WO_6 material with high interfacial lattice matching.[46] As displayed in Fig. 4f, the well-connected and matched interfacial lattice facilitates charge carrier transfer between components, leading to a significant enhancement in the CO_2 photoreduction performance of the heterojunction photocatalyst. The yields of CO and CH_4 increased substantially compared to those with the original catalyst (Fig. 4g). Owing to the average carrier lifetime of CuS–Bi_2WO_6 being longer than that of the pristine Bi_2WO_6 nanosheets, the charge transfer and separation efficiency at the interface have been improved (Fig. 4h). Although heterojunction structures offer significant advantages in promoting charge carrier separation and transfer, their formation process presents certain challenges. For instance, suspension bonds and dislocations are prone to occur at the heterojunction interface, serving as recombination centers, which reduces the efficiency of charge carrier migration. Furthermore, enhanced charge separation may lead to electron enrichment at the reduction site, thus limiting CO_2 reduction efficiency due to insufficient proton supply. In the future, it will be crucial to select semiconductor materials with matching crystal planes to construct heterojunctions and investigate the real charge transfer mechanisms during the photoreduction process.

2.2.2 Alloy structure accelerates charge carrier separation. With the advancement of scientific research, alloying strategies have emerged as a prevalent approach to enhance

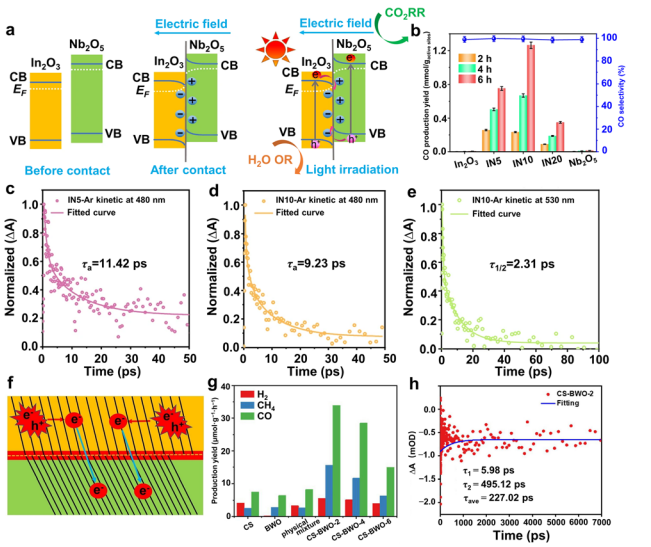

Fig. 4 (a) In_2O_3/Nb_2O_5 S-heterojunction formation and charge transfer mechanism. (b) The CO yield and selectivity of different catalysts. (c–e) Kinetic decay curves of the transient absorption spectra of different catalysts. Reproduced with permission from ref. 45. Copyright 2024, Springer Nature. (f) Scheme of a heterojunction with highly connected and matching crystal faces. (g) Product evolution rates of different catalysts. (h) Normalized transient absorption kinetics for CuS–$BiWO_6$. Reproduced with permission from ref. 46. Copyright 2024, Wiley-VCH.

photocatalytic CO_2 performance.[47–49] Researchs have demonstrated that these strategies improve photocatalytic activity by optimizing charge carrier behavior in catalysts. Furthermore, alloying strategies offer innovative methods to boost the catalytic activity and selectivity of photoreduced CO_2 by adjusting the composition of alloy phases. For instance, Guo *et al.* synthesized NiCo alloy-modified crystalline carbon nitride (CCN) (Fig. 5a).[50] The N 1s peak shift (Fig. 5b) indicated strong electronic interaction between N atoms in CCN and the NiCo alloy, which facilitated charge separation and reduced electron–hole recombination thereby enhancing photocatalytic performance. Additionally, the PL spectrum (Fig. 5c) showed that the steady-state PL emission intensity of NiCo alloy-modified CCN was significantly reduced compared to that of the unmodified CCN. The time-resolved transient PL decay spectra in Fig. 5d further confirmed that the alloy modification enhances photogenerated charge carrier separation and transfer, thus achieving the purpose of improving the photocatalytic performance. Fig. 5e demonstrated that the change in alloy composition has a significant impact on the product distribution. Co-rich alloys exhibited preferential CO generation, whereas Ni-dominant configurations favor HCOOH formation. This indicated that the compositional modulation of multi-component alloys exerted a pronounced influence on product selectivity in catalytic processes, which was predominantly governed by the interplay between electronic structure modifications, surface active site engineering, and synergistic interactions among constituent elements. Similarly, Liu *et al.* developed CuAg alloy/UiO66–NH_2 and investigated its electronic effects on enhancing photocatalytic CO_2 performance.[51] The catalyst demonstrated stable cycling performance, successfully undergoing at least five consecutive experiments while maintaining its remarkable catalytic performance (Fig. 5f). The PL spectra in Fig. 5g showed that the PL peak intensity of CuAg alloy/UiO66–NH_2 was significantly lower than that of the original sample, indicating reduced photogenerated charge carrier recombination efficiency. As displayed in Fig. 5h, the low mean relaxation time of CuAg alloy/UiO66–NH_2 indicated that the photogenerated charge carrier recombination was inhibited. Furthermore, they employed femtosecond transient absorption (Fs-TA) spectroscopy to study the photogenerated charge carrier dynamics. The results (Fig. 5i) showed that the introduction of the CuAg alloy promotes the separation of photogenerated charge carriers. Although alloying promotes the spatially effective separation of charge carriers *via* electron trapping traps and modulation of photogenerated charge carrier mobility, effectively inhibiting charge carrier recombination, clarifying the correlation between accelerated electron transfer and catalytic active sites in multi-component alloys remains challenging.

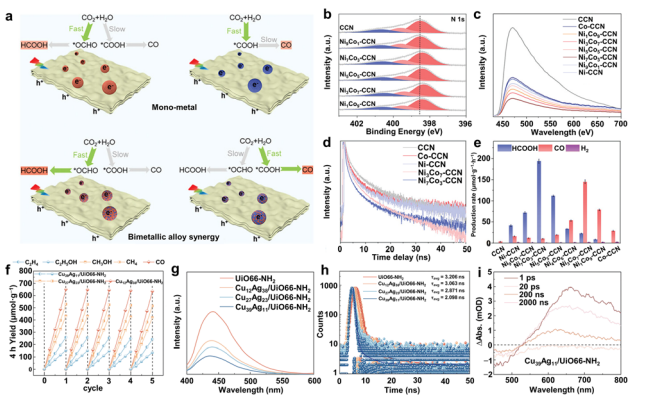

Fig. 5 (a) Schematic diagram of the reaction mechanism of photoreduction of CO_2 by the Ni_xCo_y–CCN catalyst. (b) XPS spectra of N 1s, (c) PL spectra and (d) time-resolved transient PL decay spectra for Ni_xCo_y–CCN. (e) Product evolution rates of Ni_xCo_y–CCN. Reproduced with permission from ref. 50. Copyright 2024, Wiley-VCH. (f) The cycling test over Cu_xAg_{50-x}/UiO66–NH_2. (g) PL spectra; (h) time-resolved transient PL decay spectra and (i) Fs-TA spectra of Cu_xAg_{50-x}/UiO66–NH_2. Reproduced with permission from ref. 51. Copyright 2024, Royal Society of Chemistry.

2.3 Tailoring the protonation process

2.3.1 Composite structure regulates the adsorption configuration of intermediates. The protonation process plays a crucial role in the photoreduction of CO_2, significantly influencing both reaction kinetics and product selectivity. Despite its fundamental importance, the key role of the protonation step remains underexplored in current research. Controlling the selectivity of products in photoreduced CO_2 can be effectively achieved by precisely regulating the protonation process.[11] By employing thermodynamic design of the CO_2 photoreduction process and strategic adjustment of the intermediate connection structure, the reaction pathway can be optimized to steer the formation of desired products. This approach, as demonstrated in a recent study designing the intermediate adsorption structure of M–C–O–M (where M represents the active sites on the catalyst surface), has emerged as a promising research direction and current hotspot in the field.[52,53] On this basis, our research group has developed van der Waals contact nanosheet composites, as shown in Fig. 6a. By introducing double active sites, we have successfully promoted the thermodynamic formation of CH_3OH through a novel intermediate bonding mechanism, thereby advancing the understanding and efficiency of CO_2 photoreduction.[54] The pristine In_2O_3 nanosheets

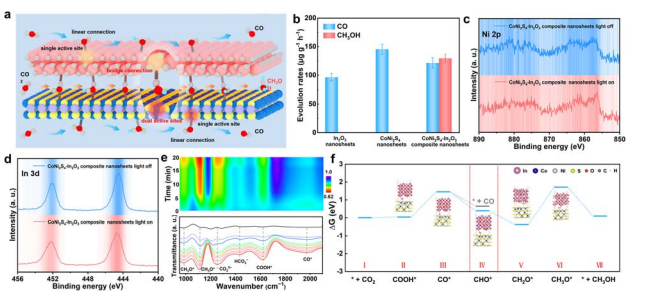

Fig. 6 (a) Schematic diagram of interlayer dual active site fixation intermediates promoting photoreduction of CO_2 to CH_3OH. (b) Rates of CO_2 photoreduction with different catalysts. Quasi *in situ* XPS spectra of (c) Ni 2p and (d) In 3d for the $CoNi_2S_4$–In_2O_3 composites of nanosheets. (e) *In situ* FTIR spectra and (f) free energy diagrams for the CO_2 photoreduction process on the $CoNi_2S_4$–In_2O_3 composite of the nanosheet slab. Reproduced with permission from ref. 54. Copyright 2024, American Chemical Society.

and $CoNi_2S_4$ nanosheets were capable of producing only a single CO product during the CO_2 photoreduction process, whereas the synthesized $CoNi_2S_4$–In_2O_3 composite nanosheets were able to produce CH_3OH, as demonstrated in Fig. 6b. By means of quasi *in situ* XPS spectra (Fig. 6c and d), it was found that both Ni and In atoms served as active sites in the CO_2 photoreduction process. More importantly, bridge-absorbed CO* intermediates were observed in the *in situ* infrared spectrum (Fig. 6e), further indicating a stable bridging effect between CO* and $CoNi_2S_4$–In_2O_3 composite nanosheets. Additionally, Gibbs free energy calculations (Fig. 6f) revealed that the COOH* formation energy of the $CoNi_2S_4$–In_2O_3 composite was significantly lower than that of $CoNi_2S_4$ and In_2O_3, suggesting that CO_2 reduction initiation on the composite is more favorable. This jointly indicated that the bridging structure of Ni–C–O–In facilitated the generation of CH_3OH as the product. In addition to designing bimetallic sites to stabilize intermediates, Wang *et al.* developed WO_3 nanosheets with surface ordered defects, demonstrating excellent photocatalytic capabilities.[55] Due to surface ordered line defects altering the surface electronic structure, the interaction between CO_2 molecules and W atoms promotes the photoreduction of CO_2 to CH_4. Consequently, regulating the connection mode of reaction intermediates can change the reaction pathway, providing a promising strategy for achieving the selective photoreduction of CO_2 to the desired hydrocarbons. Nevertheless, it remains challenging to explore the dynamic evolution of intermediates on active sites during the process. Moreover, current studies often rely on ideal surface models, whereas in actual reactions, factors such as defects and crystal planes can significantly alter the adsorption energy barriers, thus impacting experimental outcomes.

2.3.2 Loading engineering constructs charge asymmetric pair sites. The construction of bimetallic sites has been demonstrated to be an effective strategy for promoting C–C coupling.[56,57] This occurs as it enhances the interaction between the supported metal atoms and the substrate material through the introduction of heteroatoms, leading to the formation of bimetallic sites with distinct surface charge densities.[58,59] These sites result in significantly different charge distributions of adjacent C_1 intermediates, thus effectively suppressing electrostatic repulsion forces and enabling C–C coupling. As shown in Fig. 7a, our group successfully loaded Pd particles onto Nb_2O_5 nanosheets, facilitating the C–C coupling of intermediates to produce C_2 products.[60] The TEM image (Fig. 7b) confirmed the uniform loading of Pd particles on the Nb_2O_5 nanosheets. Experimental results from the photoreduction of CO_2 at atmospheric concentration demonstrated that the Pd loaded Nb_2O_5 nanosheets exhibited superior ability to convert CO_2 into C_2 products (Fig. 7c). Furthermore, the introduction of Pd particles induced an asymmetric charge distribution on the Pd–Nb_2O_5 nanoplates (Fig. 7d), supported by DFT calculations which indicated that this modification thermodynamically favorable for C_2 product formation (Fig. 7e). Building on this, our group explored Pd loading onto ZnO nanosheets in cluster form.[61] The HAADF image (Fig. 7f) revealed the presence of bright regions without lattice stripes on ZnO nanosheets, indicating Pd existed in cluster form. Quasi *in situ* XPS analysis

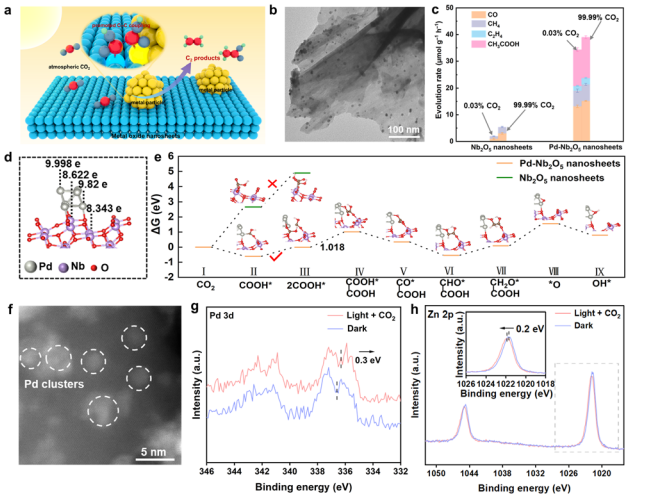

Fig. 7 (a) Schematic representation of CO_2 photoreduction in bimetallic sites. (b) TEM image of Pd–Nb_2O_5 nanosheets, (c) product evolution rates for CO_2 photoreduction over various catalysts. (d) Calculated Bader charge value for a Pd–Nb_2O_5 nanosheet slab. (e) Free energy diagrams of CO_2 photoreduction to CH_3COOH over the Pd–Nb_2O_5 nanosheets. Reproduced with permission from ref. 60. Copyright 2024, Wiley-VCH. (f) TEM of Pd–ZnO nanosheets. Quasi *in situ* XPS spectra of (g) Pd 3d and (h) Zn 2p for the Pd–ZnO nanosheets during CO_2 photoreduction. Reproduced with permission from ref. 61. Copyright 2024, Wiley-VCH.

confirmed that Pd cluster loading formed Pd–Zn bimetallic sites, thereby enhancing CO_2 photoreduction to C_2 products (Fig. 7g and h). Beyond noble metal-based catalysts,[62] the strategic construction of charge-symmetric active centers employing cost-effective non-precious metals presents significant potential for practical applications. Lau *et al.* successfully immobilized both copper nanoclusters and atomic Cu monomers on a C_3N_4 substrate through precise anchoring techniques.[63] The study revealed that adjacent Cu species exhibited robust synergistic interactions, which facilitated the highly selective photocatalytic reduction of CO_2 to CH_3CH_2OH. Furthermore, transition metal sulfides have demonstrated exceptional potential in constructing charge-asymmetric active sites for catalytic applications. Notably, Wu *et al.* engineered bimetallic Au–Mo dual sites anchored on MoS_2, which demonstrated exceptional efficacy in stabilizing critical oxygenated intermediates during the CO_2 reduction process.[64] This strategic configuration achieved a remarkable enhancement in CH_3COOH selectivity. Overall, the development of bimetallic active sites through cluster or particle loading can effectively lower the reaction energy barrier and promote C–C coupling. However, this approach still faces the challenge of C_1 and C_2 products being catalyzed simultaneously on the same metallic active site, thereby reducing selectivity.

2.3.3 Surface vacancies and hydroxyl groups produce charge asymmetric pair sites. The introduction of diverse active sites in catalytic systems can be achieved through multiple approaches.[65,66] While metal–metal active sites are commonly constructed, other charge-asymmetric active sites, such as surface vacancy-functional group sites, are also beneficial for C_2 product formation.[67] Ishihara *et al.* developed a WO_3–$0.33H_2O$

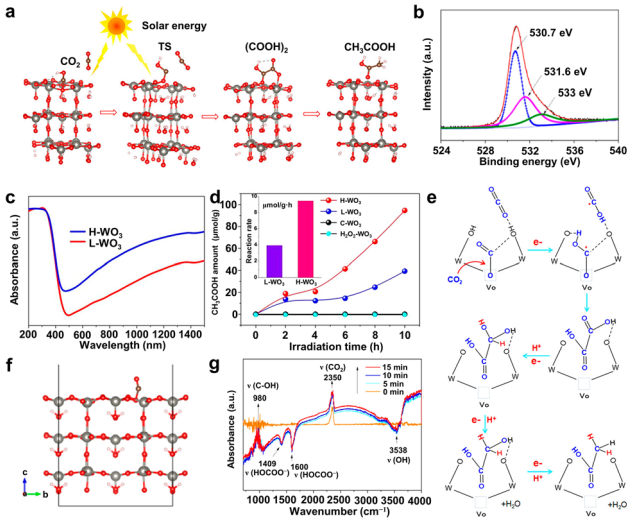

Fig. 8 (a) Schematic representation of CO_2 photoreduction in bimetallic sites. (b) O 1s XPS spectra of an H–WO_3 catalyst. (c) UV-vis-NIR absorption spectrum of catalysts. (d) CH_3COOH yield increasing with irradiation time. (e) Adsorption of CO_2 on the anoxic WO_3–$0.33H_2O$ surface. (f) *In situ* DRIFT spectrum of the H–WO_3. (g) Schematic diagram of possible reaction pathways in CH_3COOH production. Reproduced with permission from ref. 68. Copyright 2018, American Chemical Society.

catalyst featuring abundant sustainable surface Vo sites, which efficiently converted CO_2 to CH_3COOH under sunlight (Fig. 8a).[68] Fig. 8b and c demonstrated the successful synthesis of samples with higher oxygen vacancy concentrations. The CO_2 photoreduction performance tests revealed that WO_3–$0.33H_2O$ nanotubes with elevated oxygen vacancy concentrations exhibited outstanding CH_3COOH generation rates (Fig. 8d). This performance can be attributed to the presence of surface vacancies, where the positively charged Vo effectively accumulates abundant free electrons during photocatalysis, thereby increasing the surface negative charge density. This enhanced charge density facilitates CO_2 adsorption and activation, elongating the C=O bond (Fig. 8e). Furthermore, the *in situ* DRIFT spectrum (Fig. 8f) indicated that this process promotes the formation of HCO_3^- intermediates. Under illumination, when HCO_3^- was proximal to the O=COH intermediate at hydroxyl sites, spontaneous reactions occur, fostering C–C coupling (Fig. 8g). While this study highlights the synergistic effects between surface vacancies and hydroxyl groups, the research on CO_2 photoreduction remains limited in depth. Therefore, the development of a stable and sustainable synergistic photocatalyst integrating vacancy and hydroxyl functionalities holds promising prospects in promoting C–C coupling. However, the challenge of stably adsorbing hydroxyl groups to function as active sites remains to be addressed.

3 Conclusions and outlook

Comprehensive insights were presented on the rational design of photocatalyst active sites for promoting the photoreduction of CO_2 into C_1 or C_2 products. This review systematically explores strategies from three key perspectives: enhancing light absorption, accelerating charge carrier separation, and regulating the protonation process. The discussed approaches include defect structure, metal doping structure, heterojunction structure, alloy structure, loading structure, and composite structure. In detail, we outlined how defects in WO_3 nanosheets and BiOBr nanosheets can promote the generation of intermediate bands and boost the performance of the photoreduction of CO_2 to CO. We also emphasized the incorporation of Au, Pt, and Pd in BiOCl, which contributed to broadening the spectral range through their LSPR effect. Secondly, we reviewed how the In_2O_3/Nb_2O_5 heterojunction and NiCo alloy-modified CCN accelerated electron transfer and promoted charge carrier separation to enhance the photoreduction performance of CO_2. Additionally, we explored the conversion of CO_2 to CH_3OH by constructing a Ni–C–O–In adsorption structure *via* the $CoNi_2S_4$–In_2O_3 composite structure and detailed how the composite structure affects the intermediate's adsorption structure. Furthermore, we summarized that loading Pd in the form of clusters or particles on nanosheets can construct charge asymmetric pair sites, thus reducing the C–C coupling energy barrier. Despite their proven effectiveness in regulating the CO_2 photoreduction process, there remain areas requiring improvement and innovation within photocatalytic CO_2 reduction. Based on this, we propose the following recommendations for advancing the photoreduction of CO_2 into high-value products (Fig. 9).

(a) The photoreduction of CO_2 involves a multi-electron reaction process, where precise control of electron transfer to a specific step remains challenging, often resulting in poor product selectivity. To overcome these challenges, the photocatalyst must provide a favorable coordination environment that modulates the adsorption strength of intermediate products. Surface modification methods, such as adjusting the coordination number of active sites, functional group modification of the charge carrier, and introducing corresponding co-catalysts, can enhance product selectivity. These modifications alter the local electronic structure and thermodynamically reduce the adsorption energy of intermediates, thereby

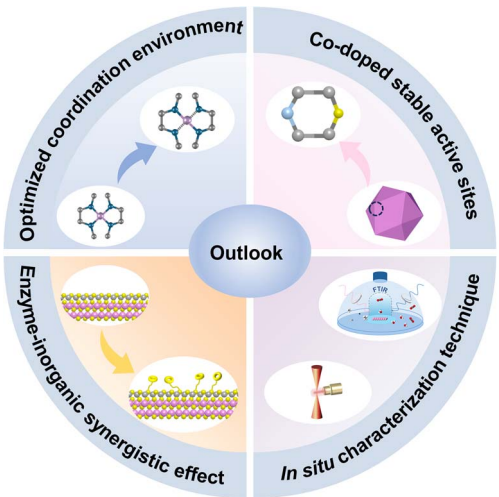

Fig. 9 Outlook on the design of active sites for CO_2 photoreduction.

regulating reaction pathways and improving product selectivity. Therefore, optimizing the surface coordination environment is a powerful approach to enhancing product selectivity.

(b) The practical application of photocatalytic CO_2 reduction is significantly hindered by insufficient catalyst stability, primarily attributed to deactivation mechanisms. Such issues include metal center agglomeration in single-atom photocatalysts during cyclic operations and rapid poisoning of Pd-based catalysts due to excessive *CO intermediate adsorption, both representing critical challenges in catalyst design. Future research should prioritize developing advanced stabilization strategies, particularly those enhancing metal–support interactions to mitigate agglomeration and preserve atomic dispersion of active sites. Furthermore, rational catalyst engineering through co-doping architectures could modulate intermediate adsorption configurations and prevent surface passivation while maintaining catalytic fidelity throughout photoreduction processes.

(c) The integration of solar catalysis with natural enzymatic processes offers a favorable model for efficient solar-to-chemical energy conversion. Biological enzymes exhibit exceptional photostability during light-driven reactions, a feature that current photocatalytic CO_2 reduction systems seek to emulate through enzyme encapsulation within engineered matrices. In the future, by developing structures that mimic the active sites of enzymes in natural photosynthesis and combining them with existing inorganic materials, a sophisticated synthesis of photocatalysts that imitate the enzyme sites can be achieved, so as to enhance the catalytic performance of photoreduction of CO_2.

(d) A thorough elucidating of the structural evolution of the active sites of photocatalysts during the photoreduction process holds paramount scientific significance. It not only provides fundamental insights into the internal processes such as adsorption and activation of the active sites during the reaction process, but also establishes a strategic framework for the rational design and performance optimization of photocatalysts. It is of critical importance to explore the reaction mechanism by employing advanced *in situ* characterization methodologies. While *in situ* XPS[62] and *in situ* infrared spectroscopy[69,70] are commonly used, other techniques like *in situ* mass spectrometry and *in situ* NMR spectroscopy[71] offer potential for deeper insights into intermediate evolution processes, thereby strengthening the theoretical foundation of the research.

In the future, efforts will be focused on elucidating the selective regulatory mechanism of the CO_2 photoreduction reaction. We aim to reveal the true reaction pathways responsible for producing C_1 or C_2 products at different sites. With a particular emphasis on the generation of high-value-added hydrocarbons such as C_2, our research will address the current limitation in the field where C_1 products predominantly dominate.

Data availability

The data supporting this article have been included within the article. No new data were generated or analysed as part of this review.

Conflicts of interest

The authors declare no competing financial interest.

Acknowledgements

This work was financially supported by the National Key R&D Program of China (2022YFA1502904), the National Natural Science Foundation of China (22275178) and the Fundamental Research Funds for the Central Universities (JUSRP123013, JUSRP123015).

References

1 K. de Kleijne, S. Hanssen, L. van Dinteren, M. A. J. Huijbregts, R. van Zelm and H. de Coninck, *One Earth*, 2022, **5**, 168–185.
2 J. Rogelj, M. den Elzen, N. Höhne, T. Fransen, H. Fekete, H. Winkler, R. S. Chaeffer, F. Ha, K. Riahi and M. Meinshausen, *Nature*, 2016, **534**, 631–639.
3 G. G. Zhang, G. S. Li, T. Heil, S. Zafeiratos, F. L. Lai, A. Savateev, M. Antonietti and X. C. Wang, *Angew. Chem., Int. Ed.*, 2019, **58**, 3433–3437.
4 Y. Tachibana, L. Vayssieres and J. R. Durrant, *Nat. Photonics*, 2012, **6**, 511–518.
5 D. Gust, T. A. Moore and A. L. Moore, *Acc. Chem. Res.*, 2009, **42**, 1890–1898.
6 Y. Hao and A. Steinfeld, *Sci. Bull.*, 2017, **62**, 1099–1101.
7 T. Zhang and W. B. Lin, *Chem. Soc. Rev.*, 2014, **43**, 5982–5993.
8 J. Jia, H. Wang, Z. L. Lu, P. G. O'Brien, M. Ghoussoub, P. Duchesne, Z. Q. Zheng, P. C. Li, Q. Qiao, L. Wang, A. Gu, F. M. Ali, Y. C. Dong, Q. Wang, K. K. Ghuman, T. Wood, C. X. Qian, Y. Shao, C. Y. Qiu, M. M. Ye, Y. M. Zhu, Z. H. Lu, P. Zhang, A. S. Helmy, C. V. Singh, N. P. Kherani, D. D. Perovic and G. A. Ozin, *Adv. Sci.*, 2017, **4**, 1700252.
9 L. Hurtado, R. Natividad and H. García, *Catal. Commun.*, 2016, **84**, 30–35.
10 R. Das, S. Chakraborty and S. C. Peter, *ACS Energy Lett.*, 2021, **6**, 3270–3274.
11 Q. Y. Hu, M. Q. Li, J. C. Zhu, Z. X. Zhang, D. P. He, K. Zheng, Y. Wu, M. H. Fan, S. Zhu, W. S. Yan, J. Hu, J. F. Zhu, Q. X. Chen, X. C. Jiao and Y. Xie, *Nano Lett.*, 2024, **24**, 4610–4617.
12 Y. Wang, S. B. Wang and X. W. Lou, *Angew. Chem., Int. Ed.*, 2019, **58**, 17236–17240.
13 Y. Wu, Q. X. Chen, J. C. Zhu, K. Zheng, M. Y. Wu, M. H. Fan, W. S. Yan, J. Hu, J. F. Zhu, Y. Pan, X. C. Jiao, Y. F. Sun and Y. Xie, *Angew. Chem., Int. Ed.*, 2023, **62**, e202301075.
14 S. Chakraborty, R. Das, M. Riyaz, K. Das, A. K. Singh, D. Bagchi, C. P. Vinod and S. C. Peter, *Angew. Chem., Int. Ed.*, 2023, **62**, e202216613.
15 A. Corma and H. Garcia, *J. Catal.*, 2013, **308**, 168–175.
16 J. Y. Liu, B. Garg and Y. C. Ling, *Green Chem.*, 2011, **13**, 2029–2031.
17 X. C. Jiao, K. Zheng, L. Liang, X. D. Li, Y. F. Sun and Y. Xie, *Chem. Soc. Rev.*, 2020, **49**, 6592–6604.

18 M. Q. Li, Z. Q. Han, Q. Y. Hu, W. Y. Fan, Q. Hu, D. P. He, Q. X. Chen, X. C. Jiao and Y. Xie, *Chem. Soc. Rev.*, 2024, **53**, 9964–9975.
19 S. W. Wang, J. S. Wang, Y. Wang, X. Y. Sui, S. H. Wu, W. X. Dai, Z. Z. Zhang, Z. X. Ding and J. L. Long, *ACS Catal.*, 2024, **14**, 10760–10788.
20 Y. Wu, Q. Hu, Q. Chen, X. Jiao and Y. Xie, *Acc. Chem. Res.*, 2023, **56**, 2500–2513.
21 J. Albero, Y. Peng and H. García, *ACS Catal.*, 2020, **10**, 5734–5749.
22 G. R. Dey, *Petroleum*, 2024, **10**, 373–398.
23 A. Behera, A. K. Kar and R. Srivastava, *Mater. Horiz.*, 2022, **9**, 607–639.
24 S. W. Cheng, Z. H. Sun, K. H. Lim, T. Z. H. Gani, T. X. Zhang, Y. S. Wang, H. Yin, K. L. Liu, H. W. Guo, T. Du, L. Y. Liu, G. K. Li, Z. Y. Yin and S. Kawi, *Adv. Energy Mater.*, 2022, **12**, 2270079.
25 H. B. He, Y. Q. Ren, Y. H. Zhu, R. X. Peng, S. N. Lan, J. C. Zhou, B. Y. Yang, Y. T. Si and N. X. Li, *ACS Catal.*, 2025, **15**, 10480–10520.
26 C. Han, B. K. Kundu, Y. J. Liang and Y. J. Sun, *Adv. Mater.*, 2024, **36**, e2307759.
27 S. Yang, W. J. Byun, F. Zhao, D. Chen, J. Mao, W. Zhang, J. Peng, C. Liu, Y. Pan, J. Hu, J. Zhu, X. Zheng, H. Fu, M. Yuan, H. Chen, R. Li, M. Zhou, W. Che, J.-B. Baek, J. S. Lee and J. Xu, *Adv. Mater.*, 2024, **36**, 2312616.
28 L. Liang, X. D. Li, Y. F. Sun, Y. L. Tan, X. C. Jiao, H. X. Ju, Z. M. Qi, J. F. Zhu and Y. Xie, *Joule*, 2018, **2**, 1004–1016.
29 J. C. Wu, J. C. Zhu, W. Y. Fan, D. P. He, Q. Y. Hu, S. Zhu, W. S. Yan, J. Hu, J. F. Zhu, Q. X. Chen, X. C. Jiao and Y. Xie, *Nano Lett.*, 2024, **24**, 696–702.
30 Y. Wu, D. P. He, L. Li, Z. Q. Wang, W. S. Yan, J. F. Zhu, Y. Pan, Q. X. Chen, X. C. Jiao and Y. Xie, *Chem. Commun.*, 2023, **59**, 11700–11703.
31 J. Wu, X. D. Li, W. Shi, P. Q. Ling, Y. F. Sun, X. C. Jiao, S. Gao, L. Liang, J. Q. Xu, W. S. Yan, C. M. Wang and Y. Xie, *Angew. Chem., Int. Ed.*, 2018, **57**, 8719–8723.
32 T. Y. Huang, J. Y. Han, Z. Q. Li, Y. X. Hong, X. F. Gu, Y. F. Wu, Y. J. Zhang and S. Q. Liu, *Angew. Chem., Int. Ed.*, 2025, **64**, e202500269.
33 X. Y. Jiang, J. D. Huang, Z. H. Bi, W. J. Ni, G. Gurzadyan, Y. A. Zhu and Z. Y. Zhang, *Adv. Mater.*, 2022, **34**, 2109330.
34 M. Tahir, B. Tahir and N. A. S. Amin, *Appl. Catal., B*, 2017, **204**, 548–560.
35 L. Z. Shi, H. M. Liu, S. B. Ning and J. H. Ye, *Catal. Sci. Technol.*, 2022, **12**, 6155–6162.
36 C. Boerigter, R. Campana, M. Morabito and S. Linic, *Nat. Commun.*, 2016, **7**, 10545.
37 R. T. Guo, C. Xia, Z. X. Bi, Z. R. Zhang and W. G. Pan, *Fuel Process. Technol.*, 2023, **241**, 107617.
38 Q. Liu, C. B. Bai, C. X. Zhu, W. J. Guo, G. F. Li, S. Guo, D. Kripalani, K. Zhou and R. Chen, *Adv. Sci.*, 2024, **11**, 2400934.
39 N. Y. Huang, B. Li, D. J. Wu, Z. Y. Chen, B. Shao, D. Chen, Y. T. Zheng, W. J. Wang, C. Z. Yang, M. Gu, L. Li and Q. Xu, *Angew. Chem., Int. Ed.*, 2024, **63**, e202319177.
40 W. D. Hou, H. Z. Guo, M. H. Wu and L. Wang, *ACS Nano*, 2023, **17**, 20560–20569.
41 W. Gui, S. Jiang, L. Wang, C. Liu, Z. Huang, L. Wang and J. Yang, *Adv. Funct. Mater.*, 2025, 2505919.
42 Z. L. Liu, Y. F. Mu, X. R. Li, Y. X. Feng, M. Zhang and T. B. Lu, *Appl. Catal., B*, 2025, **366**, 125012.
43 D. Liu, L. Jiang, D. Chen, Z. Hao, B. Deng, Y. Sun, X. Liu, B. Jia, L. Chen and H. Liu, *ACS Catal.*, 2024, **14**, 5326–5343.
44 R. Sun, Z. Zhu, N. Tian, Y. Zhang and H. Huang, *Angew. Chem., Int. Ed.*, 2024, **63**, e202408862.
45 X. Y. Deng, J. J. Zhang, K. Z. Qi, G. J. Liang, F. Y. Xu and J. G. Yu, *Nat. Commun.*, 2024, **15**, 4807.
46 J. Tian, Y. Zhang, Z. Shi, Z. Liu, Z. Zhao, J. Li, N. Li and H. Huang, *Angew. Chem., Int. Ed.*, 2025, **64**, e202418496.
47 X. Wang, H. H. Liao, W. Tan, W. Song, X. Li, J. W. Ji, X. Q. Wei, C. Wu, C. X. Yin, Q. Tong, B. Peng, S. C. Sun, H. Q. Wan and L. Dong, *ACS Appl. Mater. Interfaces*, 2024, **16**, 22089–22101.
48 B.-H. Yan, B.-R. Xu, Y. Jin, H. Xiao, S.-C. Luo, R.-H. Duan, H. Li, X.-Q. Yan, B. Lin and G.-D. Yang, *cMat*, 2024, **1**, e28.
49 H. W. Huang, J. W. Zhao, H. L. Guo, B. Weng, H. W. Zhang, R. A. Saha, M. L. Zhang, F. L. Lai, Y. F. Zhou, R. Z. Juan, P. C. Chen, S. B. Wang, J. A. Steele, F. L. Zhong, T. X. Liu, J. Hofkens, Y. M. Zheng, J. L. Long and M. B. J. Roeffaers, *Adv. Mater.*, 2024, **36**, 2313209.
50 X. F. Kang, Z. Z. He, F. Wang, Y. Liu and L. J. Guo, *Adv. Funct. Mater.*, 2025, **35**, 2419802.
51 L. P. Jiang, D. Q. Chen, Z. K. Hao, D. X. Cao, R. Q. Liu, J. Y. Cheng, L. M. Chen, X. Liu, B. Y. Jia and D. D. Liu, *Energy Environ. Sci.*, 2024, **17**, 8228–8242.
52 Y. Chai, Y. H. Kong, M. Lin, W. Lin, J. N. Shen, J. L. Long, R. S. Yuan, W. X. Dai, X. X. Wang and Z. Z. Zhang, *Nat. Commun.*, 2023, **14**, 6168.
53 X. Zhu, Y. Cao, Y. Song, J. Yang, X. She, Z. Mo, Y. She, Q. Yu, X. Zhu, J. Yuan, H. Li and H. Xu, *Small*, 2021, **17**, 2103796.
54 J. C. Wu, F. Huang, Q. Y. Hu, D. P. He, W. X. Liu, X. D. Li, W. S. Yan, J. Hu, J. F. Zhu, S. Zhu, Q. X. Chen, X. C. Jiao and Y. Xie, *J. Am. Chem. Soc.*, 2024, **146**, 26478–26484.
55 S. K. Xue, C. G. Wei, M. Shen, X. C. Liang, J. L. Wang, C. Yang, W. D. Xing, S. B. Wang, W. Lin, Z. Y. Yu, Y. D. Hou, J. C. Yu and X. C. Wang, *Proc. Natl. Acad. Sci. U. S. A.*, 2024, **121**, e2319751121.
56 W. W. Shao, X. D. Li, J. C. Zhu, X. L. Zu, L. Liang, J. Hu, Y. Pan, J. F. Zhu, W. S. Yan, Y. F. Sun and Y. Xie, *Nano Res.*, 2022, **15**, 1882–1891.
57 L. Cheng, X. Y. Yue, L. X. Wang, D. N. Zhang, P. Zhang, J. J. Fan and Q. J. Xiang, *Adv. Mater.*, 2021, **33**, e2105135.
58 H. N. Shi, H. Z. Wang, Y. C. Zhou, J. H. Li, P. L. Zhai, X. Y. Li, G. G. Gurzadyan, J. G. Hou, H. Yang and X. W. Guo, *Angew. Chem., Int. Ed.*, 2022, **61**, e202208904.
59 C. Chen, C. Ye, X. Zhao, Y. Zhang, R. Li, Q. Zhang, H. Zhang and Y. Wu, *Nat. Commun.*, 2024, **15**, 7825.
60 J. Y. Ding, P. J. Du, P. P. Li, W. X. Liu, J. Q. Xu, W. S. Yan, Y. Pan, J. Hu, J. F. Zhu, Q. X. Chen, X. C. Jiao and Y. Xie, *Angew. Chem., Int. Ed.*, 2025, **64**, e202414453.

61 P. Du, J. Ding, C. Liu, P. Li, W. Liu, W. Yan, Y. Pan, J. Hu, J. Zhu, X. Li, Q. Chen and X. Jiao, *Angew. Chem., Int. Ed.*, 2025, **64**, e202421353.
62 G. Wang, Z. Chen, T. Wang, D. S. Wang and J. J. Mao, *Angew. Chem., Int. Ed.*, 2022, **61**, e202210789.
63 Z. Guo, H. Yang, X. Huang, Y. Ning, H. Luo, J. Xie, J. He, Y. Liu and T.-C. Lau, *Angew. Chem., Int. Ed.*, 2025, e202423666.
64 C. Chen, C. Ye, X. Zhao, Y. Zhang, R. Li, Q. Zhang, H. Zhang and Y. Wu, *Nat. Commun.*, 2024, **15**, 7825.
65 J. Ding, P. Du, J. Zhu, Q. Hu, D. He, Y. Wu, W. Liu, S. Zhu, W. Yan, J. Hu, J. Zhu, Q. Chen, X. Jiao and Y. Xie, *Angew. Chem., Int. Ed.*, 2024, **63**, e202400828.
66 W. Gao, L. Shi, W. Hou, C. Ding, Q. Liu, R. Long, H. Chi, Y. Zhang, X. Xu, X. Ma, Z. Tang, Y. Yang, X. Wang, Q. Shen, Y. Xiong, J. Wang, Z. Zou and Y. Zhou, *Angew. Chem., Int. Ed.*, 2024, **63**, e202317852.
67 L. Zhang, T. Liu, T. Liu, S. Hussain, Q. Li and J. Yang, *Chem. Eng. J.*, 2023, **463**, 142358.
68 S. M. Sun, M. Watanabe, J. Wu, Q. An and T. Ishihara, *J. Am. Chem. Soc.*, 2018, **140**, 6474–6482.
69 Y. Wu, Q. X. Chen, J. C. Zhu, K. Zheng, M. Y. Wu, M. H. Fan, W. S. Yan, J. Hu, J. F. Zhu, Y. Pan, X. C. Jiao, Y. F. Sun and Y. Xie, *Angew. Chem., Int. Ed.*, 2023, **62**, e202301075.
70 H. Huang, J. Zhao, B. Weng, F. Lai, M. Zhang, J. Hofkens, M. B. J. Roeffaers, J. A. Steele and J. Long, *Angew. Chem., Int. Ed.*, 2022, **61**, e202204563.
71 K. Zheng, S. Y. Liu, J. C. Zhu, Z. Q. Dai, C. Y. Liu, B. W. Li, Y. B. Zheng, X. Y. Chen, L. Zhai, Y. Wu, W. X. Liu, M. H. Fan, J. Hu, Y. Pan, J. F. Zhu, F. F. Sun, Y. F. Sun and Y. Xie, *Angew. Chem., Int. Ed.*, 2025, e202508259.